Automated Design of CLLLC Resonant Converters Based on Time-Domain Model

Felix Woltjen
KOSTAL Automobil Elektrik GmbH & Co. KG
Dortmund, Germany
f.woltjen@kostal.com

Krishna Kumar Narayanan
KOSTAL Eléctrica, S. A.
Barcelona, Spain
k.narayanan@kostal.com

Manuel Kracht
KOSTAL Automobil Elektrik GmbH & Co. KG
Dortmund, Germany
m.kracht@kostal.com

2024 Energy Conversion Congress & Expo Europe (ECCE Europe) | 979-8-3503-6444-6/24/$31.00 ©2024 IEEE | DOI: 10.1109/ECCEEurope62508.2024.10751986

***Abstract*—This paper demonstrates how metaheuristic methods can be used to find optimal design parameters for power electronic converters. The method will be applied to the CLLLC resonant converter, a popular choice for bidirectional applications such as battery chargers. This topology is a complex system that requires a time-consuming design process, which is why developers often resort to simplifications, including first harmonic approximation or design constraints. However, these methods lack accuracy or drastically limit the solution space. In this paper, the time-domain model of the CLLLC resonant converter will be used to obtain accurate calculation results, while an optimization algorithm determines component values in an automated manner. It will be shown that significant improvements can be achieved for a given converter specification and reference design.**

***Index Terms*—clllc, resonant converter, time-domain model, automated design, optimization, metaheuristic algorithms**

I. Introduction

With the goal of reducing electricity generation from fossil fuels globally, there is a growing need for bidirectional power flow converters to locally support the grid with decentralized energy storage systems such as electric vehicles (EV). In order to deliver electrical energy from the battery to the grid, the onboard charger (OBC) of the EV generally includes a bidirectional dc-dc converter with galvanic isolation. Resonant dc-dc converters are a popular choice due to their inherent soft-switching capability and therefore high efficiency [1], [2]. While the well established LLC resonant converter is sufficient for unidirectional operation, an additional resonant element has to be added to achieve bidirectional power flow in a feasible manner [1], [2] (Fig. 1). This further increases the complexity of the system, which is why a prevalent design approach is to simplify the analysis by using the first harmonic approximation (FHA) [3]. While this approach allows for a fast assessment, it is inaccurate for frequencies considerably smaller or larger than the resonance frequency [4]. Another common approach is to choose the component values in such a manner, that the resonance frequency on the primary and secondary side are identical [5]. This method greatly simplifies the analysis in the time-domain, whilst giving accurate results. However, due to the wide voltage range of an OBC, a restriction of the design space is not practical because it leads to nonoptimal solutions [6], [7]. Instead of solving the system of differential equations analytically, it is also possible to use circuit simulation software. While being very accurate, this approach is very time-consuming even for a reasonable solution space [7]. In addition, the simulation has to reach it's steady state first, which increases the computation time even further. Sophisticated cloud computing with parallel simulation execution is needed to make this approach feasible [7]. In [4], a novel time-domain model (TDM) for the CLLLC is introduced. The model can be used to accurately calculate voltage and current waveforms for asymmetrical configurations, even if the switching frequency greatly diverts from the resonance frequency. The work also defines critical design parameters which are then used to determine suitable component values. Such conventional design of power electronics involves careful selection of component values based on expert knowledge, with some design features being discrete in nature (e.g. switches), while others are continuous (e.g. switching frequency). The complexity increases rapidly with the number of considered components, features and optimization objectives, which makes manually finding a global optimum unrealistic. Application of Artificial Intelligence (AI) methods for such design processes is an active area of applied research and alleviates this problem [8]–[10]. Metaheuristic methods belong to a family of algorithms inspired from biology, which arrive at the optimal family of solutions by evolving a subset of initial candidates. In this paper, the proposed TDM of [4] is adapted and used in an alternative design approach based on metaheuristic methods. In section II, the basic equations of the model are shown and calculation results verified. In section III, the implemented design tool structure and design methodology are explained. Optimization results are discussed in section IV. It will be shown that the TDM can be used to design an asymmetrical CLLLC in a feasible amount of time.

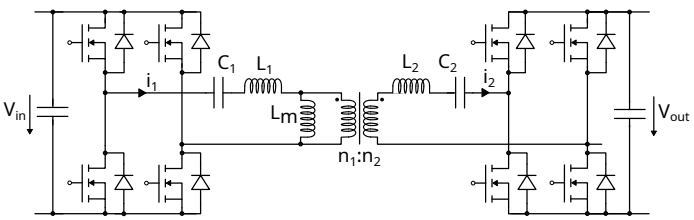

Fig. 1: CLLLC resonant converter circuit diagram.

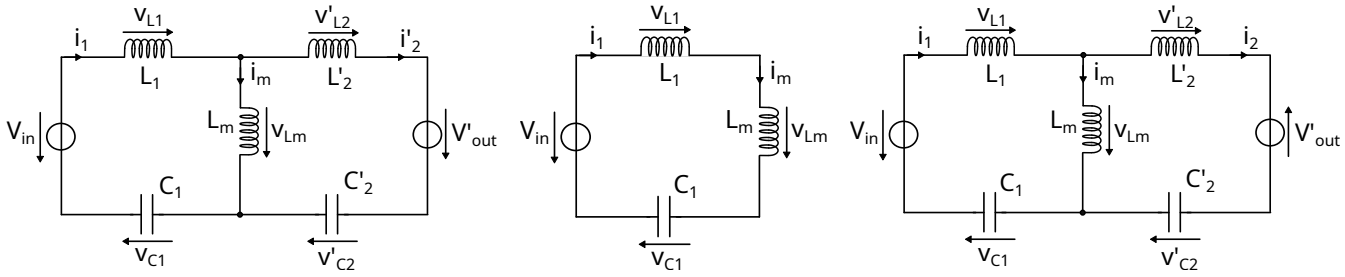

(a) P-state (b) 0-state (c) N-state

Fig. 2: Primary side equivalent circuits for each CLLLC resonant state [4], [5].

II. Converter Modelling

A. Parameter conversion

According to [4], the CLLLC can be categorized as S-type ($L_1C_1 = L_2C_2$), D-type ($L_1C_1 \neq L_2C_2$), asymmetric ($L_1 \neq n^2L_2$, $C_1 \neq C_2/n^2$) and symmetric ($L_1 = n^2L_2$, $C_1 = C_2/n^2$) with $n = n_1/n_2$. In order to make the analytical calculation of the asymmetric D-type feasible, a parameter conversion to S-type is proposed in [4]. After converting the component values with (1)-(10), the resulting S-type circuit has the same terminal voltages and input respectively output current waveforms [4].

$$H_l = L_2/L_1 \tag{1}$$

$$K_a = L_1/L_m \tag{2}$$

$$H_c = C_1/C_2 \tag{3}$$

$$e_0 = \sqrt{4n^2H_c + (1 + n^2H_lK_a - n^2H_c(1 + K_a))^2} \tag{4}$$

$$L_{1,S} = L_1 \cdot (1+n^2(H_c+(H_c+H_l)K_a)-e_0)/(2n^2H_cK_a) \tag{5}$$

$$L_{2,S} = L_1 \cdot (1+n^2(H_c+(H_c+H_l)K_a)-e_0)/(2n^2K_a) \tag{6}$$

$$L_{m,S} = L_1 \cdot (-1+n^2(H_c+(H_c-H_l)K_a)+e_0)/(2n^2H_cK_a) \tag{7}$$

$$C_{1,S} = C_1 \tag{8}$$

$$C_{2,S} = C_2 \tag{9}$$

$$n_S = (-1 + n^2(H_c + (H_c - H_l)K_a) + e_0)/(2nH_c) \tag{10}$$

Solely the voltages of the magnetic components and the magnetizing current are different to the original D-type and have to be converted back after calculation of the S-type waveforms [4].

B. Time-Domain Model

The time-domain behaviour of the CLLLC can be described by three characteristic resonant stages [5]. In the P-state, the rectifying bridge voltage is clamped to $+V_{out}$ (Fig. 2a). When in 0-state, there is no current flowing on the rectifying side (Fig. 2b). In the N-state, the rectifying bridge voltage is clamped to $-V_{out}$ (Fig. 2c). Within a single period, the converter can go through multiple resonant stages e.g. PN, 0P0, N0P etc. generally known as operation modes. In [4], 14 operation modes have been identified, of which not all are practical. In order to express the time-domain behaviour of the converter, the system of differential equations for each resonant state has to be solved. By using equivalent circuits (Fig. 2), equations for each state can be established. Solving the P-state system (11) gives expressions for $i_{1,P}(t)$, $i_{2,P}(t)$, $u_{1,P}(t)$ and $u_{2,P}(t)$. Similarly, (12) can be solved to obtain the 0-state equations. For the N-state, simply substitute $-V_{out}$ for V_{out} in the P-state solutions. By applying boundary conditions of continuity and periodicity, e.g. $i_{1,P}(T_p) = i_{1,0}(T_0)$, with T_p being the end of the P-state and T_0 being the start of the 0-state, a system of non-linear equations with unknown initial conditions can be established for each operation mode. With the exception of single-stage operation modes such as P or 0, the equations have to be solved numerically for their initial conditions [4], [5], which requires high computational effort.

$$\begin{aligned} L_m\frac{di_m}{dt} + L_1\frac{di_1}{dt} + v_{C1} &= V_{in} \\ L_m\frac{di_m}{dt} - L_2'\frac{di_2'}{dt} - v_{C2}' &= V_{out}' \\ i_1 = C_1\frac{dv_{C1}}{dt}, i_2' &= C_2\frac{dv_{C2}'}{dt} \\ i_1 &= i_2 + i_m \end{aligned} \tag{11}$$

$$\begin{aligned} L_m\frac{di_m}{dt} + L_1\frac{di_1}{dt} + v_{C1} &= V_{in} \\ i_1 = C_1\frac{dv_{C1}}{dt}, i_2 = 0, i_1 &= i_m \end{aligned} \tag{12}$$

C. Model Verification

To verify the correct implementation of the proposed calculation method, the results have been compared with LTspice circuit simulations. Because all resistances and parasitic effects are neglected in the TDM, these influences have also been omitted in the simulation model. Furthermore, the battery side full-bridge is assumed to be an ideal rectifier for charging operation. Likewise, the grid side is operating as ideal rectifier for vehicle-to-grid operation. Fig. 3 shows a comparison of calculated and simulated waveforms for an arbitrary resonant tank and operating point (OP). It can be seen that the calculated waveform aligns perfectly with the simulation result. Subsequently, this example resonant tank has been simulated for a set of OPs to verify the model for the whole operating

area. Fig. 4 shows the voltage gain $M = nV_{out}/V_{in}$ for several input powers over the normalized switching frequency $f_n = f_{sw}/f_{res}$ with $f_{res} = (2\pi\sqrt{L_{1,S}C_{1,S}})^{-1}$. The results confirm that the implemented model is accurate over the whole operating range, even when the switching frequency greatly diverts from the resonance.

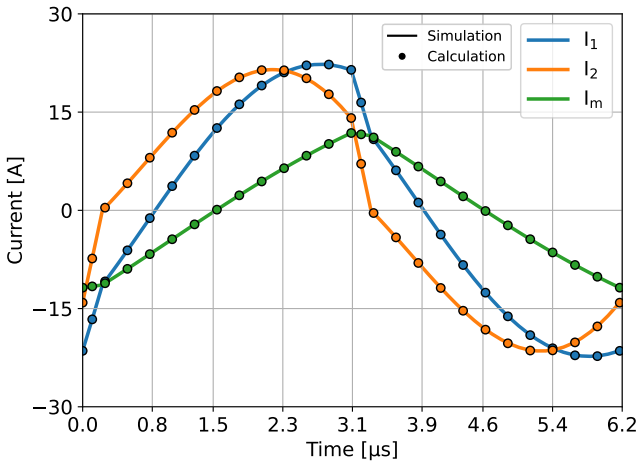

Fig. 3: Calculated waveforms of I_1, I_2, I_m compared with simulated waveforms for an arbitrary asymmetrical resonant tank. $V_{in} = 800$V, $V_{out} = 500$V, $P_{in} = 7.2$kW, $f_{sw} = 161$kHz.

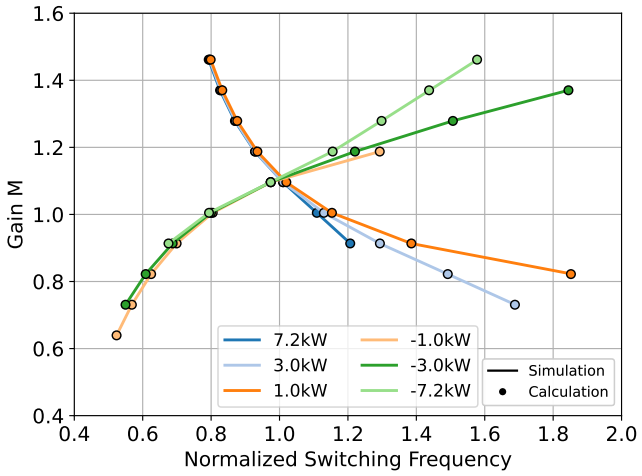

Fig. 4: Comparison of calculated and simulated gain for an arbitrary asymmetrical resonant tank over several operating points for $V_{in} = 800$V and $f_{res} = 130$kHz.

On an average developer PC with a 16-core 5.4GHz CPU, the implemented calculations run at 18 OP per second. The implemented simulation on the other hand runs at 2 OP per second, mainly due to the fact that it has to come to an equilibrium state first. Both methods can be further accelerated by using multiple cores simultaneously, which has been made use of for the following design process.

III. Converter Design

A. Design Tool

The CLLLC TDM is integrated into an in-house power electronics design tool built for designing and evaluating power electronic products consisting of multiple topologies which can be connected series or parallel. Fig. 5 illustrates the hierarchical structure of the design tool: product level, topology level, component level and database. In a first step, the product is fed by (customer) requirements such as derating, voltage, temperature and power ranges. From these requirements, a sufficient number of OPs, including but not limited to critical OPs, is generated in order to evaluate the product in terms of feasibility and efficiency over the whole operating area. The topology level, which could consist of a single topology or multiple topologies in series and/or parallel, is then calculated for all the generated OP with component currents, voltages, etc. being stored. In turn, the underlying component level, i.e. semiconductors, inductive components, capacitors, etc. uses the data to calculate component losses and temperatures with basic thermal models. Database level information from datasheets, measurements or even custom behaviour is used by components. This allows the application to also take switch performance into account, which can be difficult for simulations due to convergence problems in certain operating points, while also slowing down the simulation. Lastly, all the generated output data can be post processed to generate standardized plots. For demonstration purposes, $N_{SW} = 5$ arbitrary switches ($R_{ds,on}$, E_{on}, E_{off}), $N_T = 328$ transformers (L_m, n_1, n_2, A_{fe}, V_{fe}), $N_L = 245$ inductors (L_s, n, A_{fe}, V_{fe}) and $N_C = 42$ capacitors (C, R_{ESR}) with volume and cost information have been created on database level and will be used for the design process. Because primary and secondary side can make use of different components, this leads to $N_{SW1} \cdot N_{L1} \cdot N_{C1} \cdot N_T \cdot N_{L2} \cdot N_{C2} \cdot N_{SW2} = 8.68 \times 10^{11}$ combinations. While cost and volume information for

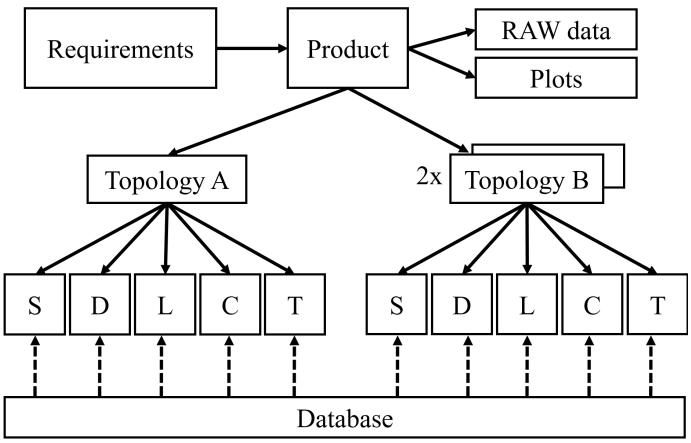

Fig. 5: Power electronics design tool structure consisting of product level, topology level, component level (switches, diodes, inductors, capacitors, transformers) and database level.

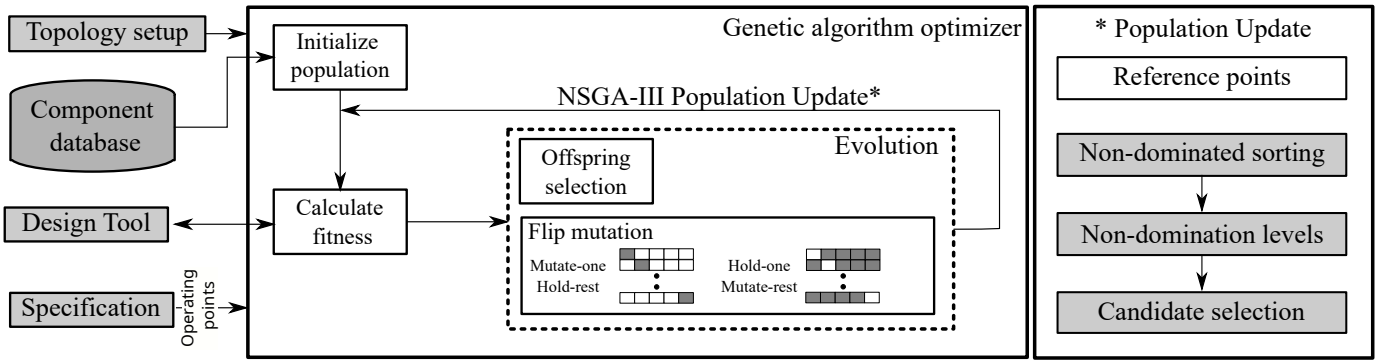

Fig. 6: Optimization framework for design optimization. Operating points for fitness evaluation are generated from a given product specification. The population is initialized using the components available in the design database. Fitness evaluation is performed using the design tool. Based on the fitness, a new population for the next generation is selected through a modified flip mutation namely mutate-one, hold-rest and hold-one, mutate-rest strategy.

each component are known from database entries, losses are estimated with help of analytical models for each OP. Switch losses consist of conduction losses $P_c = R_{ds,on}(T) \cdot I^2_{sw,RMS}$ and switching losses $P_{sw} = f_{sw} \cdot (E_{on}(T, I_{on}) + E_{off}(T, I_{off}))$, whereas diode losses are represented by $P_d = V_f(T) \cdot I_{avg} + R_d(T) \cdot I^2_{RMS}$. Losses of magnetic components include core losses calculated with the improved Generalized Steinmetz Equation (iGSE) [12] and AC winding losses $P_w = R_w(f_{sw}) \cdot I^2_{RMS}$. Capacitor losses are compromised of ESR losses $P_{ESR} = R_{ESR}(f_{sw}) \cdot I^2_{RMS}$. Current and switching frequency values are taken from the ideal waveforms calculated with the lossless TDM.

B. Design Procedure

The aforementioned design tool is used inside an optimization loop to automate the design process. Due to the high number of possible combinations, a metaheuristic selection algorithm inspired by natural selection is implemented. Fig. 6 shows the optimization framework used in this paper. The optimization function is multiple-objective and includes the maximum power loss over all OPs, total cost and total volume of the components. The Non-dominated Sorting Genetic Algorithm III (NSGA-III) [11] is used for population selection at every generation. The algorithm uses a set of pre-defined reference points distributed on a unit hyperplane. These points guide the selection process and maintain diversity in the solution space. At each iteration, the population R_t, which is a combination of the current generation P_t and the mutated offspring candidates Q_t, is sorted into levels $F_1, F_2, ..., F_n$ using the principle of non-dominated sorting [11]. This means that candidates in level F_1 are non-dominated by any other solution and levels $F_2, F_3, ..., F_n$ are dominated only by their preceding levels. The new population is then selected in a hierarchical manner until the desired population number is achieved. Because of various parameter constraint violations such as thermal runaway or insufficient gain, a large majority of the candidates is invalid. The exact number of individuals with such constraint violations is unknown beforehand without performing simulation or calculation. In order to accelerate the optimization process, a reference individual is designed manually via means of FHA and simulation and is seeded as the first individual of the population, while the rest of the generation is randomized. If no initial reference is given, all individuals of the first generation are randomized. Due to the large pool of combinations, it is possible that no valid solution is included in an entirely random population, which causes the next generation to be completely randomized as well. This process continues until at least one valid individual is found, to which mutation strategies will be applied. It is therefore advisable, but not necessary, to provide an initial solution. For a valid individual of gene length n, two mutation strategies namely hold-one, mutate-rest $(n-1)$ and mutate-one, hold-rest $(n-1)$ are used. Thus, given a valid individual of length n, $2 \times n$ offsprings are generated. The mutation also works

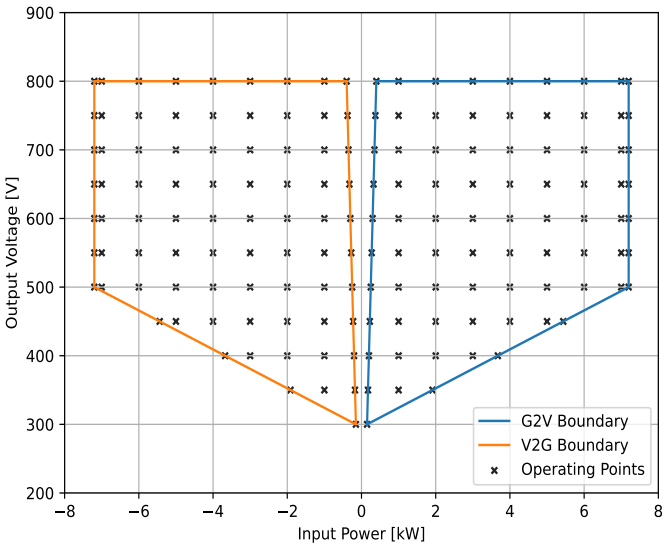

Fig. 7: Operating range V_{out} over P_{in} for $V_{in} = 800$V with OP used as input for the genetic algorithm optimizer.

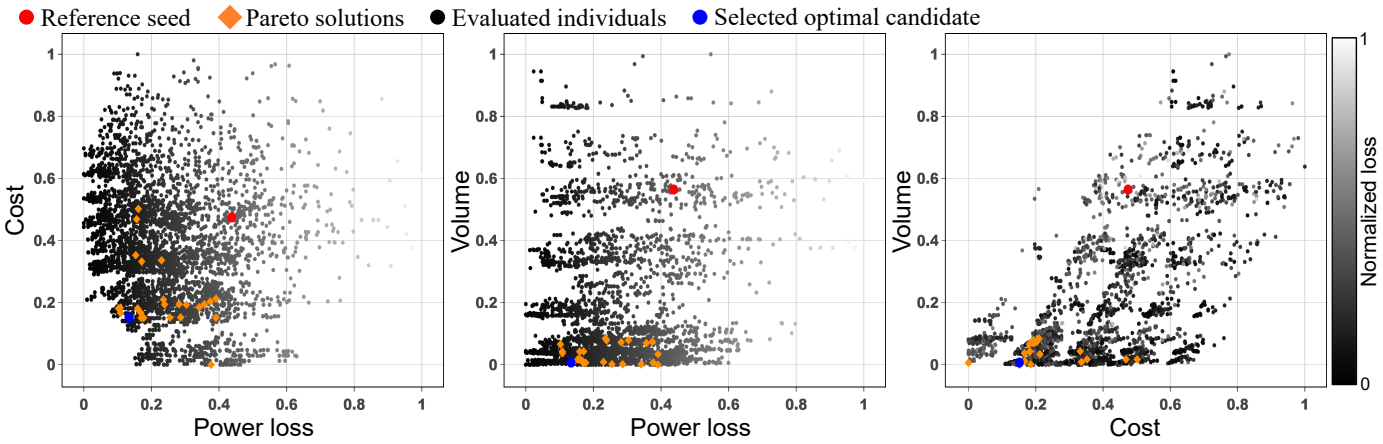

Fig. 8: Optimizer results with all valid individual combinations, reference point, corresponding Pareto front and a selected optimum from the Pareto front. The axis values are in min-max normalized space and colors of the candidates correspond to the sum of the three normalized objectives. Color scale serves only for visualization purposes.

as a cross-over, where one generates multiple variations of a given valid gene in its feature neighborhood, thereby allowing diversity in the population. Once the child designs have been created, a tournament selection based on dominance followed by elitism is implemented to form the next generations' individuals. The tournament based selection is performed by running multiple tournaments of size 2 within a set of parents and children to find individuals that dominate the majority of the population. If there are two individuals that do not inter-dominate, then the selection is based on their distance to the nearest identified neighboring solutions, also called as Crowding Distance. It is computed as the average distance between an individual and its closest n neighbors in the solution space. The one with the largest distance is selected for the next generation, thereby pushing for population diversity and promoting a balanced exploration of the search space. Elitism on the other hand is performed by picking up the individuals with the best fitness and removing those with the worst. Fig. 7 shows the operating area V_{out}, P_{in} at constant $V_{in} = 800$V and the 158 evaluated OPs for each individual. An individual will be discarded if a single OP can not be satisfied in terms of e.g. gain or thermal limits.

IV. Results

The optimization loop finished after 3 hours with 26400 calculated individuals after 60 generations, which means only 0.00003‰ of all possible combinations have been evaluated. Fig. 8 shows the valid individuals and the Pareto optimal solutions along the three objectives. It can be seen that, compared to the initial reference, individuals with considerably lower power loss, volume and cost have been found. Note that only the runtime is influenced by the initial reference and that the global optima will be found regardless of which initial design has been given to the optimizer. A comprehensive design report is created which involves a detailed breakdown of each individuals properties such as RMS currents, switching frequency, cost, volume etc. The report can easily be imported into the design tool for further evaluation to select a suitable solution. For comparison with the reference, an individual from the Pareto front has been chosen. Fig. 9 shows the gain curve of both resonant tanks. The maximum frequency at nominal power is 23% smaller for the chosen solution, which reduces switching losses and high frequency conduction losses in the magnetic components. In addition, the resulting gain is more balanced around unity due to a more favorable transformer ratio.This also reduces the worst case current stress, which can be seen in Fig. 10. A reduction of 22% for the primary side current I_1 and 15% for the secondary side current I_2 is achieved. Compared to the manually designed reference, the chosen solution reduces the volume by 67%, the cost by 25% and the worst case power losses by 27%. Because the implemented TDM assumes a lossless

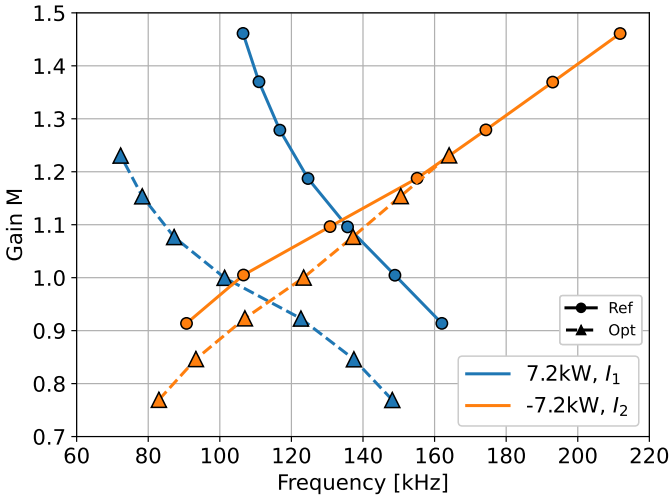

Fig. 9: Gain curve of reference and chosen Pareto optimal resonant tank at nominal power for bidirectional operation. The worst case frequency is considerably smaller for the optimized tank.

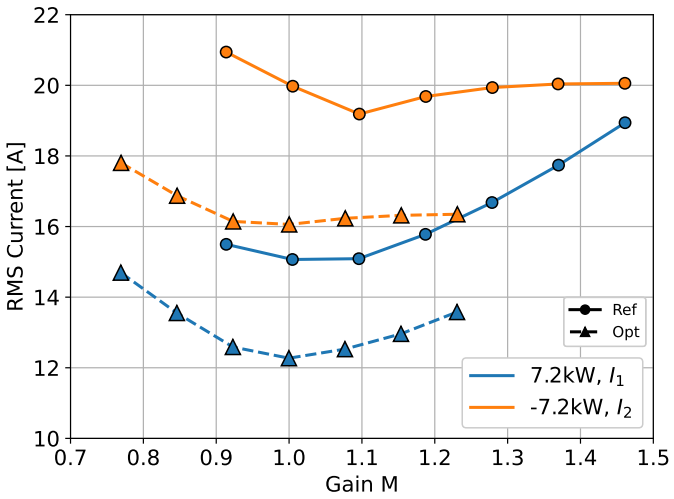

Fig. 10: RMS current values of reference and chosen Pareto optimal resonant tank at nominal power for bidirectional operation. The worst case RMS currents are considerably smaller for the optimized tank.

circuit, the gain curve of the actual application will differ from calculation. This will be most noticeable in regions with high gain slope. To address this problem, the model could be extended to include parasitic resistances, making it more complicated and increasing computational effort. Circuit simulation with parasitic elements could be used as well, but simulation time will be increased even further. It is therefore preferable to find a suitable initial design with the implemented method first, to then further improve the parameters with help of simulation and experiments.

V. Conclusion

It has been shown that the TDM of the CLLLC can be used to find optimal parameters for given converter requirements in a feasible amount of time with the help of metaheuristic methods. The optimizer can also be used to improve already implemented solutions. Furthermore, the introduced methodology is not limited to one topology, but can be extended to include any power converter model.

References

[1] W. Chen, P. Rong, Z. Lu, "Snubberless Bidirectional DC–DC Converter With New CLLC Resonant Tank Featuring Minimized Switching Loss," IEEE Transactions on Industrial Electronics, Vol. 57, No. 9, September 2010

[2] J.-H. Jung, H.-S. Kim, et al, "Design Methodology of Bidirectional CLLC Resonant Converter for High-Frequency Isolation of DC Distribution Systems," IEEE Transactions on Power Electronics 28, April 2013.

[3] L. Zheng, Y. Xiangwu, et al, "Mode analysis and optimum design of bidirectional CLLC resonant converter for high-frequency isolation of DC distribution systems," 2015 IEEE Energy Conversion Congress and Exposition, September 2015.

[4] L. Zhao, Y. Pei, L. Wang, et al, "Design Methodology of Bidirectional Resonant CLLC Charger for Wide Voltage Range Based on Parameter Equivalent and Time Domain Model," IEEE Transactions on Power Electronics, vol. 37, pp. 12041–12064, October 2022.

[5] K. Siebke, R. Mallwitz, "Operation Mode Analysis of the CLLC Resonant Converter," 2019 IEEE 13th International Conference on Compatibility, Power Electronics and Power Engineering, April 2019.

[6] J. Min, M.Ordonez, "Bidirectional Resonant CLLC Charger for Wide Battery Voltage Range: Asymmetric Parameters Methodology," IEEE Transactions on Power Electronics, vol. 36, no. 6, pp. 6662–6673, Jun. 2021.

[7] S. Ditze, S. Ehrlich, D. Happel, A. Rosskopf, "Asymmetric Resonant Tank Design for a Bidirectional CLLC Resonant Converter in G2V and V2G Operation," IEEE Applied Power Electronics Conference and Exposition, 2023.

[8] S. Estefany De Len-Aldaco, H. Calleja,J.-A. Alquicira. "Metaheuristic Optimization Methods Applied to Power Converters: A Review,´ ´ IEEE Transactions on Power Electronics 30.12, pp. 6791–6803, 2015.

[9] N. Rashidi et al. "Multi-objective Design and Optimization of Power Electronics Converters With Uncertainty Quantification Part I: Parametric Uncertainty," IEEE Transactions on Power Electronics 36.2, pp. 1463–1474, 2021.

[10] S. Zhao, F. Blaabjerg, H. Wang, "An Overview of Artificial Intelligence Applications for Power Electronics," IEEE Transactions on Power Electronics 36.4, pp. 4633–4658, 2021.

[11] K. Deb, H. Jain, "An Evolutionary Many-Objective Optimization Algorithm Using Reference-Point-Based Nondominated Sorting Approach, Part I: Solving Problems With Box Constraints," IEEE Transactions on Evolutionary Computation 18.4, pp. 577–601, 2014.

[12] J. Mühlethaler, J. Bielay, J. W. Kolar, A. Ecklebez, "Improved Core Loss Calculation for Magnetic Components Employed in Power Electronic Systems," IEEE Transactions on Power Electronics 27.2, pp. 964-973, 2012.